Journal of Catalysis 276 (2010) 201–214

Contents lists available at ScienceDirect

Journal of Catalysis

journal homepage: www.elsevier.com/locate/jcat

Nitrogen-doped titanium dioxide visible light photocatalyst: Spectroscopic identification of photoactive centers

Zizhong Zhang, Xuxu Wang, Jinlin Long *, Quan Gu, Zhengxin Ding, Xianzhi Fu *

Research Institute of Photocatalysis, State Key Laboratory Breeding Base of Photocatalysis, Fuzhou University, Fuzhou 350002, China

ARTICLE INFO

Article history:
Received 29 April 2010
Revised 27 July 2010
Accepted 29 July 2010
Available online 4 November 2010

Keywords:
Nitrogen doping
TiO_2
Photocatalyst
Visible light
Acetone
Photoactive centers

ABSTRACT

This paper focuses on the photoactive centers of nitrogen-doped TiO_2 visible light photocatalyst. A series of N-doped TiO_2 materials were prepared by a post-nitridation route at the temperature range of 400–800 °C. The photocatalytic oxidation of acetone as a model reaction was used to evaluate the photocatalytic properties of the materials. The chemical states of doped nitrogen species were characterized by near-edge X-ray absorption fine structure, X-ray photoelectron, and electron paramagnetic resonance spectroscopies. The results reveal that four types of N species exist alone or together in TiO_2 depending on nitridation temperature. The photoactive centers of the materials are a diamagnetic [$O–Ti^{4+}–N^{3-}–Ti^{4+}–V_0^-$] cluster containing an oxygen vacancy and a nitrogen anion. The visible light photocatalysis of N-doped TiO_2 is proposed to be initiated by an excited state of the surface [$Ti^{4+}–N^{3-}$] unit.

1. Introduction

Metal and nonmetal doping is a popular method to modify inorganic semiconductors, which was used widely for the preparation of visible light–responsive photocatalysts from the wide bandgap semiconductor TiO_2 [1–3]. Metal and nonmetal ions are either incorporated into bulk of the substrate or highly dispersed on surface of the substrate as clusters or as mononuclear complexes, depending on the preparation methods. As a result, the electronic structure and energy band gap of the substrate can be tuned by controlling doping conditions. It was well established that doping some metal cations such as Cr, V, and Fe and nonmetal anions including N, C, S, I, and B was able to extend the photoresponse of semiconductors to the visible light region and thus made them working under visible light [4–7]. However, unlike TiO_2, the visible light catalysts prepared by doping ions have no commonality in photocatalysis. Some such catalysts for the degradation of organic pollutants are active in an aqueous medium and yet inert in gas phase. More abstrusely, some supported-type catalysts such as ln VO_4/TiO_2 and $LaVO_4/TiO_2$ reported recently by our group are active only for certain type of reactants under visible light irradiation [8,9]. Insight into the inherent relationship between the photocatalytic function and the chemical states of dopants has been a focus of attention in photocatalysis community.

N-doped TiO_2 is the most typical example of the photocatalysts. Since it was found to be an effective visible light photocatalyst for the decomposition of pollutants by Asahi et al. in 2001 [3], the concerned study has received durative attention as reflected by the increasing archive documents [10,11]. There are large numbers of reports on the identification of N species doped in TiO_2 and the preparation of the photocatalyst by various routes [12–16], but two aspects of debates are still alive: One is the chemical states and local environment of doped nitrogen atoms. Sato et al. [14] reported that the calcination of titanium hydroxide with NH_4Cl or NH_4OH caused the photocatalytic sensitization of TiO_2 into the visible light region, and believed that the spectral sensitization of TiO_2 was originated from NO_x impurity. Asahi et al. [3] proposed that nitrogen doped into substitutional sites of TiO_2 is indispensable for bandgap narrowing and photocatalytic activity, based on density functional theory (DFT) calculations and X-ray photoelectron spectroscopy (XPS) characterization. Chen and Bruda [17] assumed N doping in the form of O–Ti–N in light of XPS results, where N-doped TiO_2 was prepared by direct treatment of TiO_2 nanocolloid with alkylammonium salts. Diwald et al. [18] doped TiO_2 (1 1 0) single crystals with nitrogen via a NH_3 treatment at 870 K. They pointed out that nitrogen is bound to hydrogen as NH_x species in interstitial sites. Reyes–Garcia et al. [16] utilized ^{15}N solid-state nuclear magnetic resonance (SSNMR) and electron paramagnetic resonance (EPR) spectroscopies to characterize N-doped TiO_2 photocatalysts and claimed that nitrogen atoms are doped in interstitial sites as nitrate species. Hitherto, all studies on the N-doped TiO_2 materials have not demonstrated completely the exact chemical

* Corresponding authors. Fax: +86 591 83738608.
E-mail addresses: jllong@fzu.edu.cn (J. Long), xzfu@fzu.edu.cn (X. Fu).

0021-9517/$ - see front matter © 2010 Elsevier Inc. All rights reserved.
doi:10.1016/j.jcat.2010.07.033

states of N species responsible for visible light photocatalysis. The main reason for the debate rests with the fact that no single spectroscopic technique (e.g. UV–vis DRS, EPR, XPS) can definitively distinguish between substitutional and interstitial N species in N-doped TiO_2 photocatalysts.

Another concerns the visible light response and the nature of visible light photocatalysis. Some studies proposed that the red-shift of optical absorption is originated from a narrowing of the band gap of pristine TiO_2 [3], whereas other studies suggested that it is due to the occurrence of intragap localized states of the dopant [11]. Serpone [19] argued on the issue concerning the origin of the spectral bands in visible absorption spectra of visible light-active TiO_2 and thought that the visible absorption bands are associated with oxygen vacancies (*F*-type color centers), whereas Chen et al. [20] reported that after reannealling in static air at 400 °C, surface oxygen vacancies were reduced considerably and the activity of N-doped TiO_2 was enhanced fourfold instead. It suggested that oxygen vacancies are not responsible for the visible light activity. It was generally admitted that nitrogen incorporation in TiO_2 introduces the chromophore that can absorb visible light, but two confusions concerning the N-doped TiO_2 visible light photocatalyst still need to be clarified: what is responsible for the visible light response? What is responsible for the visible light photocatalysis? The definitive elucidation of these scientific issues must be dependent on the well-defined identification of all nitrogen species doped in TiO_2.

A significant advance toward a clarification of the second scientific debate has been recently achieved by Livraghi et al. [21]. They used EPR technique and DFT calculations to analyze in detail the origin of photoactivity of N–TiO_2 under visible light and proposed that N_b species are responsible for visible light absorption with promotion of electrons from the bandgap localized states to the conduction band or to surface-adsorbed electron scavengers. However, conclusive evidence for the geometric structure of the N_b species has not been provided, and the relationship between the N_b species and visible light activity has not been established. The main objective of the present study is to unravel the geometric structure of photoactive N species and thus gain a deeper insight into the visible light photoexcitation and photocatalysis of N-doped TiO_2.

In this work, we firstly prepared the series of N-doped TiO_2 materials by a post-nitridation route and then the local structure of N species doped in TiO_2 was characterized in detail by ultraviolet–visible diffuse reflectance (UV–vis DRS), EPR, XPS, and near-edge X-ray absorption fine structure (NEXAFS) spectroscopies. Acetone decomposition was used as a model reaction to examine the visible light photocatalytic reactivity of these N-doped TiO_2 catalysts. The characterization results reveal clearly that the photoactive centers of N-doped TiO_2 are a diamagnetic $[O–Ti^{4+}–N^{3-}–Ti^{4+}–V_0^-]$ cluster containing an oxygen vacancy and a nitrogen anion, which acts as a source for the photogenerated electron transfer to reducible adsorbates like O_2. A synergistic effect of N dopant and oxygen vacancy on TiO_2 contributes to the great enhancement of the visible light photoactivity.

2. Experimental

2.1. Catalyst preparation

Titanium dioxide samples were synthesized by a sol–gel technique. A specific amount of titanium ethoxide was dissolved in redistilled ethanol to get a concentration of 0.1 mol L^{-1}. The precursor solution was added dropwise into water to hydrolysis under vigorous stirring. The amorphous precipitates were washed with distilled water, dried at 80 °C, and then calcined at 450 °C for 20 h in a flowing O_2 to remove residual organic compounds. The as-prepared TiO_2 was nitrified in pure NH_3 gas stream at 400, 450, 500, 550, 650, 700, or 800 °C for 20 h to produce N-doped TiO_2 samples (designated as TN-*n*, *n* = 400, 450, 500, 550 650, 700, and 800).

2.2. Catalyst characterizations

The X-ray diffraction (XRD) measurements were taken on a Bruker D8 Advance X-ray diffractometer using Cu $K\alpha_1$ radiation (λ = 1.5406 Å). UV–vis DRS spectra were obtained on a Varian Cary 500 Scan UV–vis-NIR spectrophotometer using $BaSO_4$ as a reference. The N_2 absorption–desorption isotherms were determined at 77 K with a Micromeritics ASAP 2010 instrument. EPR spectra were recorded by a Bruker A-300-EPR X-band spectrometer. XPS spectra were carried out on a VG ESCALAB 250 XPS system with a monochromatized Al Ka X-ray source (15 kV 200 W 500 μm pass energy = 20 eV). All binding energies were referenced to the C 1s peak at 284.6 eV of surface adventitious carbon. The N and O K-edge XANES spectra were collected at beamline U19 of National Synchrotron Radiation Laboratory (NSRL, China).

2.3. Photocatalytic measurements

All photocatalytic reactions were carried out in a fixed-bed reactor operated in a single-pass mode. A 500-W Xe arc lamp with a 420-nm cutoff filter ($\lambda \geqslant 420$ nm) or a near single-wavelength filter centered, respectively, at 550, 520, 450, and 420 nm (their spectral distributions are shown in Fig. S1) was used as the visible light source. A 200-W Mercury–Xenon lamp equipped with two cutoff filters (310 nm < λ < 650 nm and 250 nm < λ < 400 nm) was employed as the UV light source with a center of 365 nm (the spectral distribution is shown in Fig. S1). The weight of catalyst (50–70 mesh) was kept at 0.40 g. Acetone was kept in ice water and bubbled with oxygen to afford a reactant stream. The flow rate of reactant stream was maintained at 20 mL min^{-1}. The initial concentrations of acetone and carbon dioxide in the stream were 540 and 0 ppm, respectively. Simultaneous determination of the concentrations of acetone and carbon dioxide was performed with an online gas chromatograph (HP6890) equipped with a flame ionization detector, a thermal conductivity detector, and a Porapak R column. Acetone was found to be stable in the catalyst-loaded reactor without visible light illumination. No degradation of acetone was observed when it was illuminated in the absence of catalyst.

3. Results

3.1. Nitrogen content of the N-doped TiO_2 samples

The content of nitrogen in the N-doped TiO_2 samples obtained at different nitridation temperatures was measured on a Vario MICRO elemental analyzer, and the results are shown in Table 1. The content of N in the N-doped TiO_2 samples (TN-400, TN-450, and TN-500) prepared below 500 °C is very low (<0.25 wt.%) and tardily increases with increasing nitridation temperature, whereas above 500 °C it increases exponentially from 0.47 wt.% (550 °C) to 2.69 wt.% (650 °C), till to 13.25 wt.% (700 °C). It is evident that the nitridation temperature is a crucial factor affecting the concentration of nitrogen doped in TiO_2 and the temperature of 500 °C may be a milestone for the incorporation of nitrogen.

3.2. Photocatalytic activity of the N-doped TiO_2 samples

Prior to characterizing the chemical states of N atoms doped in TiO_2, we evaluated the photocatalytic performance of these as-prepared N-doped TiO_2 samples under visible light irradiation ($\lambda \geqslant 420$ nm) using the gas-phase photocatalytic oxidation of ace-

Table 1
BET specific surface area, nitrogen content, and surface O/Ti and N/Ti atomic ratio for the parent TiO_2 and the TN-*n* samples.

Entry	TiO_2	TN-400	TN-450	TN-500	TN-550	TN-650	TN-700
N content (wt.%)[a]	0.00	0.05	0.09	0.23	0.47	2.69	13.25
S_{BET} (m^2/g)	94	93	79	66	54	35	32
O/Ti (at.%)[b]	2.6	2.4	2.3	2.1	2.0	1.9	1.2
N1/Ti (at.%)[b]	–	2.0	2.5	3.4	1.7	1.1	0.05
N2/Ti (at.%)[b]	–	–	–	–	1.9	9.0	49.0

[a] Determined by element analysis (standard error: ⩽0.1%).
[b] Calculated from XPS spectra (standard error: ⩽10%).

tone as a model reaction. We examined emphatically the effect of nitridation time and nitridation temperature on photocatalytic activity for acetone oxidation in order to optimize the preparation conditions and to better understand the nature of visible light activity. First, we used the nitrified TiO_2 samples at 400 °C for different time as catalysts to study the photocatalytic activity as a function of nitridation time. As shown in Fig. 1, within 10 h of nitridation time, both acetone conversion and CO_2 yield monotonically increase, respectively, from 7% and 32 ppm to 10.5% and 40 ppm and finally reach a constant (10.5% of acetone conversion and 40 ppm of CO_2 yield). Based on the result, the most optimum nitridation time seems to be 20 h, where the saturated nitridation of TiO_2 can occur. Then, we studied the photocatalytic activity as a function of nitridation temperature under the indicated nitridation time (20 h) of conditions, as shown in Fig. 2. The parent TiO_2 displays a very low conversion of acetone (ca. 2.5%) and a small amount of CO_2 is produced (14 ppm). This is identical with the results reported by Suriye et al. [22], who suggested that the visible light photoactivity of the pure TiO_2 maybe originates from the existence of intrinsic defects during the long-time oxygen annealing. Compared to the pure TiO_2, the nitrified samples show a significantly enhanced photoactivity and the activity is found to be dependent on nitridation temperature. Both the acetone conversion and the CO_2 yield increase rapidly with increasing nitridation temperature and reach a maximum (ca. 17% of acetone conversion and ca. 60 ppm of CO_2 yield) at 500 °C, followed by an abrupt drop with further increasing the temperature from 550 to 800 °C. These results show that the N impurities doped in TiO_2 result in the great improvement of visible light photocatalytic performance and the optimal nitridation temperature is at 500 °C.

To confirm that the reaction is indeed induced by light absorption, we use the TN-500 sample as a model catalyst to further examine the photocatalytic activity as a function of light wavelength. As depicted in Fig. 3, the acetone conversion matches well

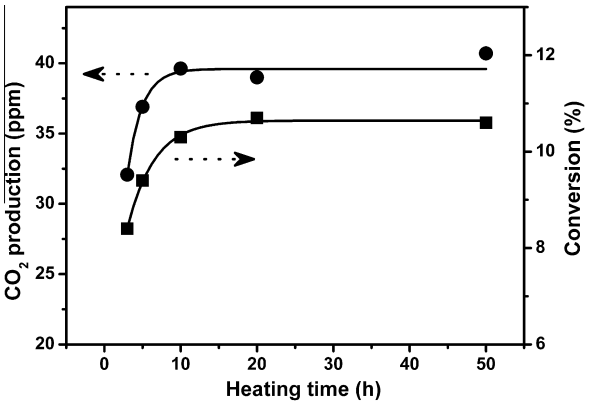

Fig. 1. Visible light photocatalytic activities for conversion of acetone and production of CO_2 on the TN-400 samples as a function of nitridation time.

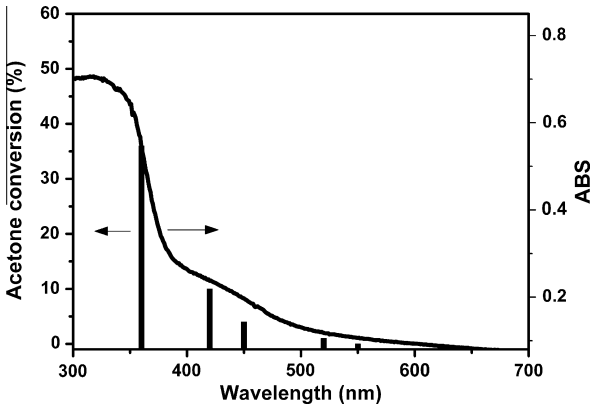

Fig. 3. Wavelength dependence of acetone conversion on the TN-500 catalyst.

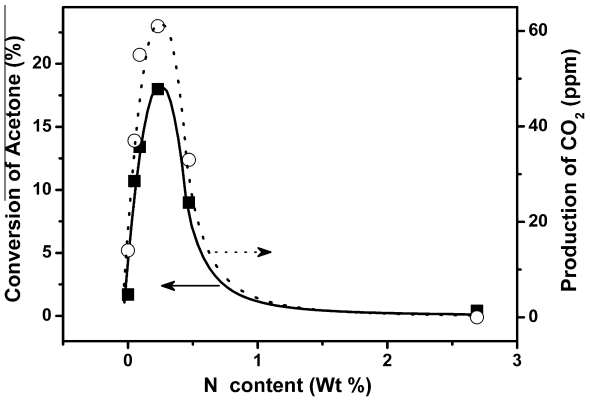

Fig. 2. Conversion of acetone and production of CO_2 versus total N content on the parent TiO_2 and the TN-*n* catalysts.

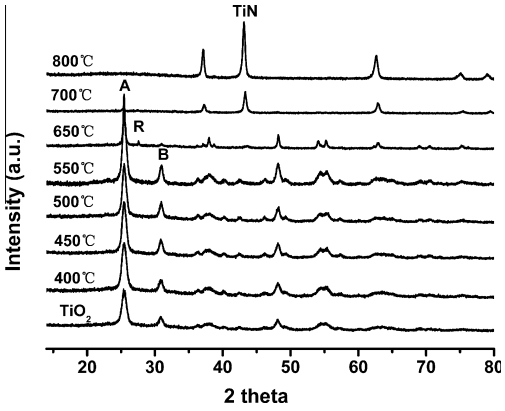

Fig. 4. XRD patterns of the parent TiO_2 and TN-*n* samples.

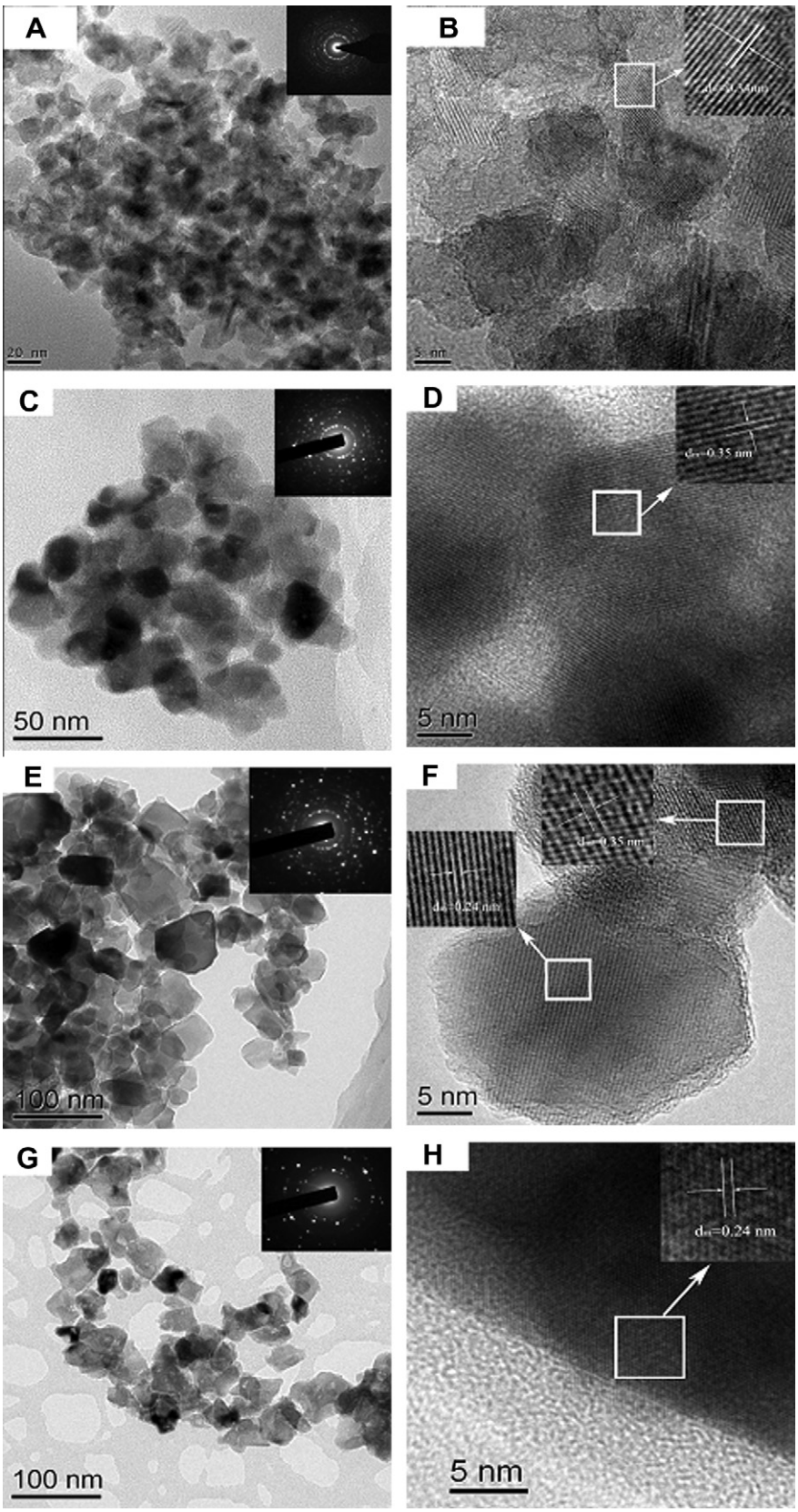

Fig. 5. TEM and HRTEM images of the parent TiO_2 (A and B), TN-500 (C and D), TN-650 (E and F), and TN-700 (G and H) samples. The insets to (A), (C), (E), and (G) show the corresponding selected area electron diffraction. The insets to (B), (D), (F), and (H) show the corresponding interplanar space.

with the diffuse reflectance spectrum of the TN-500 catalyst (The DRS spectrum will be analyzed in detail later). Above 550-nm wavelength, the catalyst is inactive due to no light adsorption. The acetone conversion on the TN-500 catalyst is ca. 35% at 365 nm, which is far lower than that (ca. 92% of acetone conversion listed in Table S1, see Supporting information) of the parent TiO_2

under the same conditions. The difference shows that N doping is deleterious to the ultraviolet (UV) light photocatalysis of TiO_2. This is quite identical with the results reported in literatures [11,14,23,24]. The origin for the sharp decrease in activity will be further discussed later.

Generally, the activity of a photocatalyst is affected by many factors such as surface area, phase structure, and crystallinity [25]. In the temperature range of 400–500 °C, although the nitridation process induces a slight increase in crystallize size of TiO_2 (the BET surface area decreases accordingly as seen from Table 1), the obtained samples still exhibit a greatly enhanced photoactivity compared to the parent TiO_2. This indicates that the texture properties of N-doped TiO_2 are not the crucial factor affecting photocatalytic properties. The nitridation above 500 °C increases significantly the content of N doped in TiO_2, but the photoactivity for acetone decomposition decreases sharply. The reason should be ascertained by identifying definitely the chemical states of N species doped in TiO_2.

3.3. Structural characteristics and optical properties of the N-doped TiO_2 samples

The crystalline structure of the parent TiO_2 and the N-doped TiO_2 samples was characterized by XRD, as shown in Fig. 4. All Bragg peaks can be well indexed to a mixed phase of anatase (A) and brookite (B) present in both the parent TiO_2 and the nitrified TiO_2 below 550 °C, but anatase is predominant (it was estimated from the peak intensity ratio that anatase accounts for 80%). The broadened diffraction peaks for the parent TiO_2 suggest that TiO_2 is in nanometric scale. The nitridation below 550 °C does not alter the crystalline phase of TiO_2 but causes the crystallite size increase due to the agglomeration of particles, as indicated by the narrowing of all Bragg peaks. This is further verified by the decrease in BET specific surface area listed in Table 1. Upon increasing nitridation temperature to 650 °C, rutile and cubic phase TiN emerge, indicating the appearance of phase transition of TiO_2 at such a temperature. The complete transformation of TiO_2 into TiN occurs at 800 °C. These XRD results indicate that the N impurities are mainly present in the form of TiN species in the N-doped TiO_2 samples obtained above 550 °C (TN-650 and TN-700) including the TN-550 sample. The TiN species are highly dispersed in the TN-550 and thus cannot be detected by XRD, which will be verified by XPS characterization below. This, together with the photoactivity result in Section 3.2, further indicates that TiN species are deleterious to the visible light photocatalysis.

The microstructural change before and after nitridation of the parent TiO_2 was further characterized by TEM, as demonstrated in Fig. 5. The TEM images of the parent TiO_2 represent stacked nanoparticles with a diameter of 18 ± 2 nm (Fig. 5A and B). After nitridation at 500 °C (Fig. 5C and D), it can be seen clearly that these nanoparticles maintain the original crystalline structure, but their size visibly increases due to conglomeration. The nitridation at high temperature of 650 °C (Fig. 5E) not only leads to the further increase in size of TiO_2 nanoparticles but also results in the formation of a small amount of TiN, as observed by HRTEM (Fig. 5F). The estimated interplanar space corresponds to a d spacing of about 0.24 nm. This is consistent with the d_{111} spacing in the XRD pattern of TiN. Upon increasing nitridation temperature to 700 °C, the TEM image (Fig. 5G) shows some particles with random shapes. A majority of TiO_2 nanoparticles are transformed into TiN (Fig. 5H). Obviously, these TEM results are in good agreement with the XRD results reported above.

The nitridation of TiO_2 extends the optical response of TiO_2 from ultraviolet to visible region. Fig. 6 shows the UV–vis DRS spectra of TN-400 samples nitrified for different time. The parent TiO_2 shows a bandedge absorption at ca. 380 nm, whereas after nitridation there occurs a broad absorption shoulder centered at about 430 nm and tailing absorption extends out to approximately 700 nm, which is the typical absorption feature reported for N-doped TiO_2 materials [11,14]. The intensity of the absorption shoulder increases with nitridation time, which is inconsistent with photocatalytic activity of TN-400 samples. No linear correlation can be established between the intensity of the optical absorption features and the photocatalytic activity. Fig. 7A displays the UV–vis DRS spectra of TiO_2 samples nitrified at the temperature range of 400–800 °C. The intensity of the absorption shoulder centered at about 430 nm increases remarkably with nitridation tem-

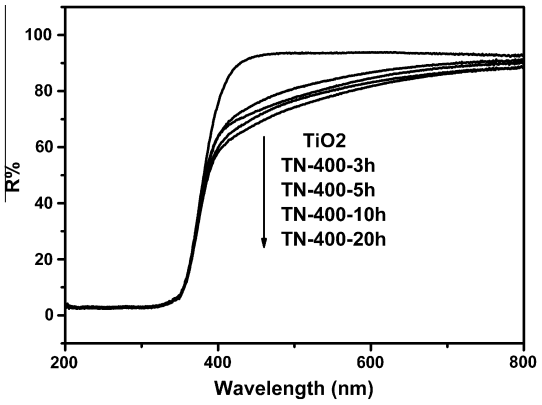

Fig. 6. UV–vis diffuse reflectance spectra of the TN-400 samples nitrified for different time.

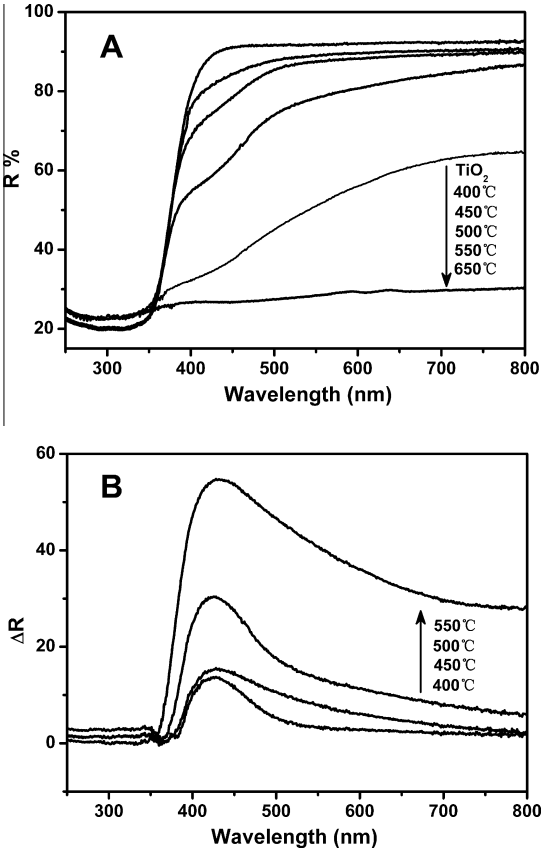

Fig. 7. (A) UV–vis diffuse reflectance spectra of the parent TiO_2 and TN-n samples. (B) The difference spectra of diffuse reflectance between the parent TiO_2 and the TN-n samples.

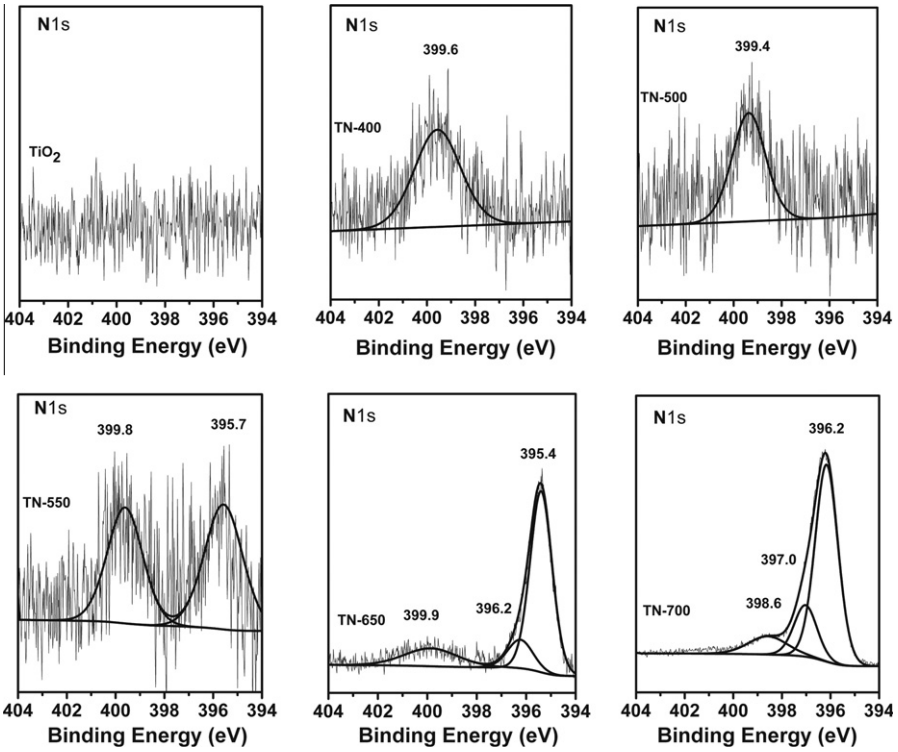

Fig. 8. N 1s XPS spectra of the TN-*n* samples.

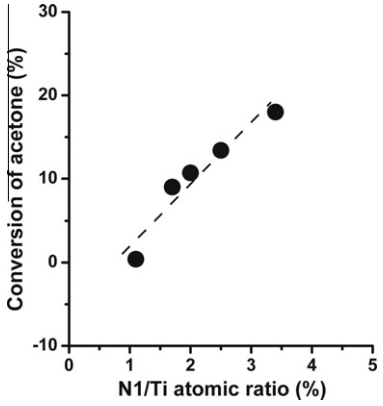

Fig. 9. Relationship between the visible light photocatalytic activities for conversion of acetone and N1/Ti atomic ratio in the N-doped TiO_2 samples.

perature as a consequence of more amounts of nitrogen doped in TiO_2. When the nitridation temperature reaches 650 °C or above, the obtained N-doped TiO_2 is not transparent in the measured regions, owing to the metallic property of formed TiN as indicated by the XRD and TEM results. The difference (ΔR) spectra between parent TiO_2 and N-doped TiO_2 ($\Delta R = R_{TiO2} - R_{NT}$) shown in Fig. 7B can more clearly demonstrate the spectral change induced by N doping. For the TN-400, TN-450, and TN-500 samples, the absorption centered at 430 nm, which arises from the contributions of doped nitrogen atoms and oxygen vacancies [11], dominates in the difference spectra and the tail absorption above 500 nm belonging to intrinsic defects such as Ti^{3+} states [26] is very weak. It shows that the nitrogen incorporation below 500 °C causes the concomitant formation of oxygen vacancies. The formed Ti^{3+} cations should be in minimum quantity and even negligible, which will be verified

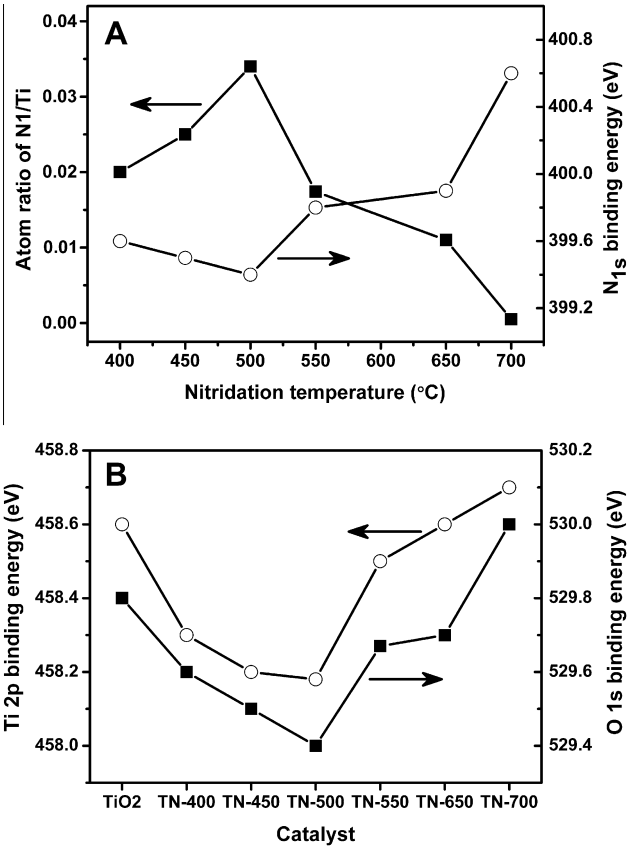

Fig. 10. (A) Dependence of N1/Ti ratio and the peak position of N1 on nitridation temperatures. (B) The peak position of O 1s and Ti 2p on pure TiO_2 and N-doped TiO_2 samples.

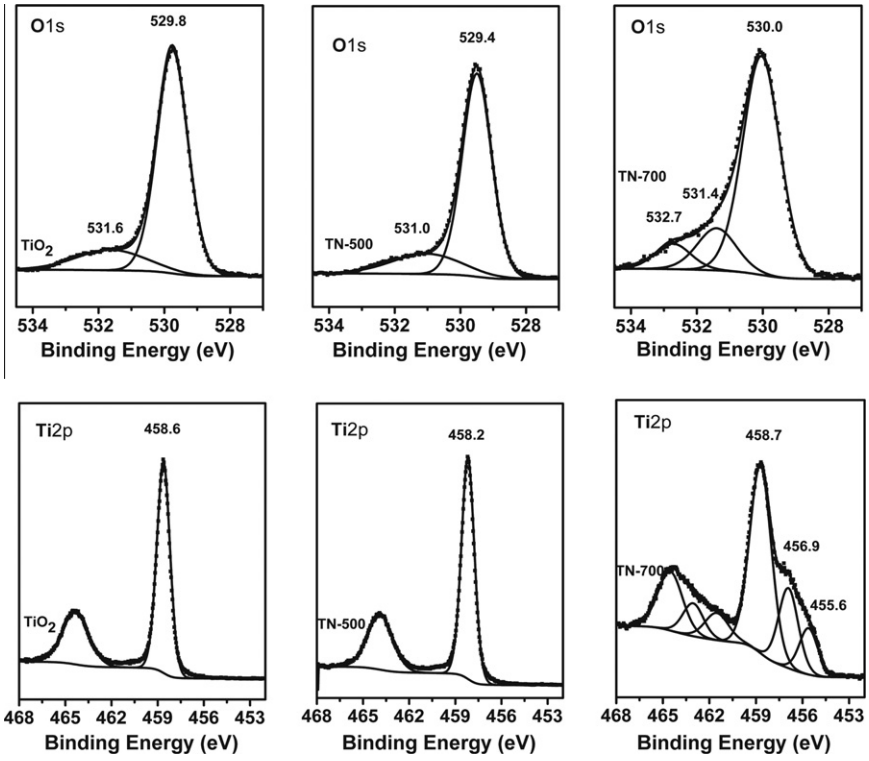

Fig. 11. O 1s and Ti 2p XPS spectra of the parent TiO_2 and TN-*n* samples.

Table 2
Peak position (eV) of O 1s and Ti $2p_{2/3}$ on pure TiO_2 and N-doped TiO_2 samples from XPS spectra.

Entry	Binding energy of O 1S			Binding energy of Ti 2P3/2		
	Peak1	Peak2	Peak3	Peak1	Peak2	Peak3
TiO_2	529.8	531.6	–	458.6	–	–
TN-400	529.6	531.6	–	458.3	–	–
TN-450	529.5	531.1	–	458.2	–	–
TN-500	529.4	531.0	–	458.2	–	–
TN-550	529.7	531.3	532.7	458.5	–	–
TN-650	529.7	531.3	532.7	458.6	457.1	–
TN-700	530.0	531.4	532.7	458.7	456.9	455.6

by EPR characterization below. However, the nitridation above 500 °C (for the TN-550 sample) makes the intensity of both the absorption centered at 430 nm and the tail absorption above 500 nm enhance significantly, showing the formation of a large amount of Ti^{3+} cations and oxygen vacancies. These UV–vis DRS results indicate that the nitridation temperature of 500 °C is a turning point. Beyond such a temperature, the chemical states of N species doped in TiO_2 start to change tremendously, which will be further validated by XPS and EPR characterizations below.

3.4. XPS analysis

The chemical states of nitrogen species in these as-prepared N-doped TiO_2 samples were further characterized by XPS, as shown in Fig. 8. The N 1s XPS spectra of the TN-400 and TN-500 samples display only one N 1s core level peak at ca. 399.5 eV, showing that the two samples contain uniform N species (denoted provisionally as N1 species). The binding energy of the N1 species is significantly lower than those of NO (402.7 eV), NO_2 (404.3 eV), and NO_3^- (407.3 eV) and yet is more close to that of NH_3 (398.7 eV) [27,28], suggesting that the valence state of the N1 species may be between −2 and −3. The unambiguous assignment to the N1 species will be discussed in detail below. For the TN-550 sample, its N 1s XPS spectrum is tremendously different from those of the TN-400 and TN-500 samples. Two N 1s core level peaks are observed at 399.8 and 395.7 eV, indicating that there exist two kinds of doped N species. This further confirms the above UV–vis DRS results. The peak at 395.7 eV should be assignable to N^{3-} bonded to three Ti atoms (denoted as N2 species) because the measured binding energy is very close to that of TiN (ca. 396.0 eV) [29]. Considering that the TN-550 sample does not show the crystalline phase of TiN in the XRD pattern, we suggested that a part of nitrogen atoms replace lattice oxygen atoms of TiO_2 to form TiN species with low nuclearity at 550 °C. Higher the nitridation temperature (above 550 °C), the more amount of nitrogen is substitutionally incorporated into TiO_2 lattice, as indicated by the most prominent N 1s peak at ca. 395.7 eV. For the TN-700 sample, the N 1s peak at ca. 399.5 eV disappears completely along with the occurrence of two new peaks at 398.6 and 397.0 eV. According to literature [29,30], the two peaks at 398.6 and 397.0 eV should belong to bulk or surface Ti–N–O species.

Surface atomic ratios of O, N1, and N2 to Ti estimated using photoelectron cross sections calculated by Scofield for these TN-*n* samples are listed in Table 1. With increasing nitridation temperature, the O/Ti atomic ratio decreases and yet the N/Ti atomic ratio increases, indicating that N atoms substitute for the surface O atoms of TiO_2. It is important to note that the N1/Ti atomic ratio reaches a maximum at 500 °C, followed by a gradual decrease. We plotted N1/Ti atomic ratio versus conversion of acetone (Fig. 9), finding a near linear correlation between them. It suggests that the N1 species are closely related with the visible light photocatalysis of N-doped TiO_2. However, the increase in the N2 species results in a considerable decrease in photoactivity, showing that the N2 species representing TiN species are deleterious to the visible light photocatalysis of N-doped TiO_2. It is identical with the above XRD results.

Additionally, it is interesting to note that the nitridation at 500 °C leads to the lowest binding energy of N1 species, as shown in Fig. 10A. The change in binding energy of N1 species is reverse to

the N1/Ti atomic ratio, i.e., the binding energy of N1 species decreases with increasing N1/Ti atomic ratio below 500 °C and then increases with decreasing N1/Ti atomic ratio. This is a very interesting result. In order to understand in depth this phenomenon, we further examined the effect of the N doping on the valence states of O and Ti atoms, as shown in Fig. 11 and Table 2. The N incorporation does induce synchronously a distinct change in the binding energies of surface O and Ti atoms of TiO_2. The TN-400 and TN-500 samples show two kinds of surface oxygen species, as observed in the O 1s spectra. A main peak belonging to the lattice oxygen atoms occurs at ca. 529.8 eV [31], and a broad peak assigned to adsorbed H_2O appears at ca. 531.6 eV [32]. For the N-doped TiO_2 samples obtained above 500 °C, beside these two oxygen species, there exists another oxygen species perhaps belonging to Ti–N–O species, as indicated by the peak at 532.7 eV. It is interesting to note that as nitridation temperature increases, the binding energy of lattice oxygen decreases gradually and reaches a bottom at 500 °C, subsequently bounces back, as indicated by Fig. 10B. These results are in parallel with the change in the binding energy of N1 species.

As such, it can be clearly seen that the Ti $2p_{3/2}$ binding energy decreases with increasing nitridation temperature and reaches a minimum at 500 °C. This also is in line with the change in the binding energy of N1 species. For the TN-550 sample, beside the Ti $2p_{3/2}$ binding energy of Ti^{4+} at 458.6 eV [31], a new and weak Ti $2p_{3/2}$ core level peak appears at 457.5 eV. According to literature [33], it is assignable to the titanium species with oxidation states between +3 and +4, which is correlated with the titanium in a distorted lattice located between the TiO_2 and TiN phases. The core level peak remarkably increases in intensity upon increasing nitridation temperature to 650 °C, indicating the increases in the titanium species. The Ti 2p spectra of the TN-700 can be fitted with three doublets corresponding, respectively, to three lower binding energies at 458.4, 456.9, and 455.6 eV. The peak at 455.6 eV is close to the published literature values for TiN phase [29]. These results indicate that the N doping below 500 °C causes the synchronous increase in the electron density of surface Ti and O atoms. Considering that the N binding energy represents the same change as those of Ti and O (Fig. 10), we proposed that the electron-donating effect may be originated from a stranger, instead of N, O, and Ti atoms. The stranger should be the concomitant oxygen vacancy during N incorporation as indicated by the UV–vis DRS spectra (Fig. 7).

3.5. NEXAFS spectroscopy

The geometry and bonding of N doping species were characterized by NEXAFS spectroscopy. Fig. 12 shows the N K-edge NEXAFS spectra of these TN-*n* samples and the reference TiN. All of N-doped TiO_2 samples represent two low energy features originating from transitions to the t_{2g} (Ti 3d + N 2pπ) and e_g (Ti 3d + N 2pσ) orbitals and higher energy features related to excitations to the N 2p and [N 2p + Ti 4sp] antibonding states. For the TN-400, TN-450 and TN-500, the spectral absorption intensity is very low due to the low content of N impurities. The strongest peak, with a broad shoulder centered at ca. 413 eV, occurs at ca. 406 eV. They arise from the transitions to hybridized orbitals involving the antibonding orbitals Ti 4sp and N 2p [34]. A stronger intensity indicates a stronger degree of interaction between N 2p and Ti 4sp orbitals. It is interesting to note that upon increasing nitridation temperature, the antibonding [Ti 4sp + N 2p] state increases visibly in intensity, showing an increase in hybridization strength of N 2p and Ti 4sp orbitals. For the nitrified samples above 500 °C, all absorption features in the NEXAFS spectra increase sharply in intensity because more amounts of N atoms are doped in TiO_2. Especially for the TN-650 and TN-700, the N K-edge spectra are highly similar to that of TiN reference, indicating that the formation of bulk-like TiN can be readily achieved above 650 °C. This is consistent with the above XRD and TEM results.

We used least-squares fit of Voigt functions and Arctan functions to further analyze the difference between these spectra. The fitting results are shown in Fig. 13. The parameters obtained

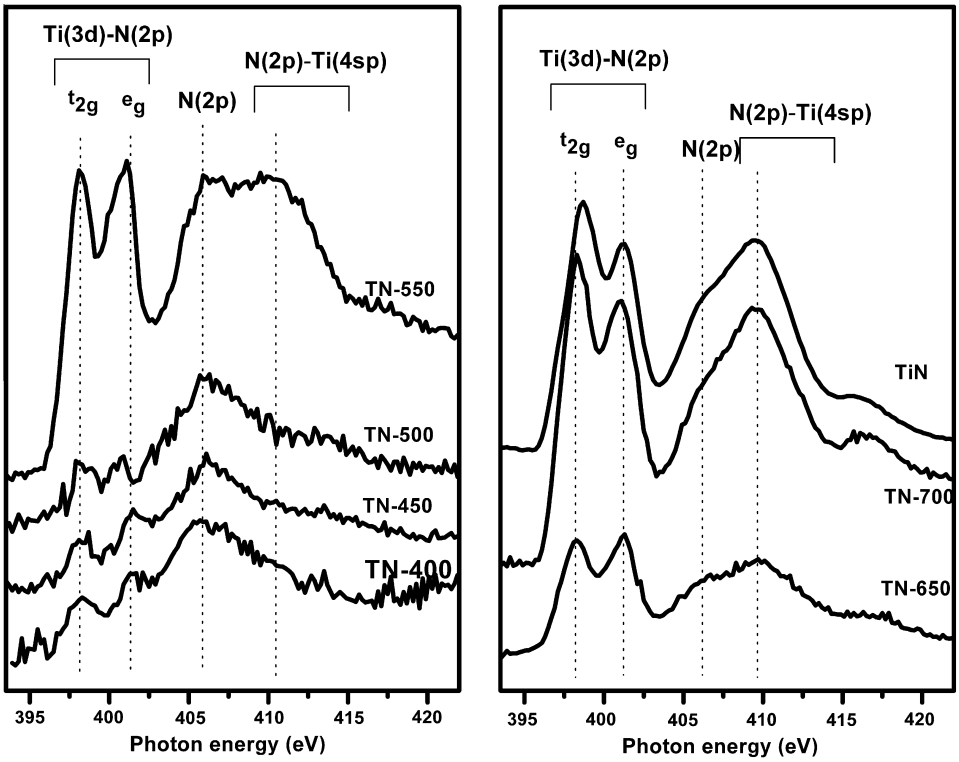

Fig. 12. NEXAFS spectra for the N K-edge of the TN-*n* samples and a TiN reference.

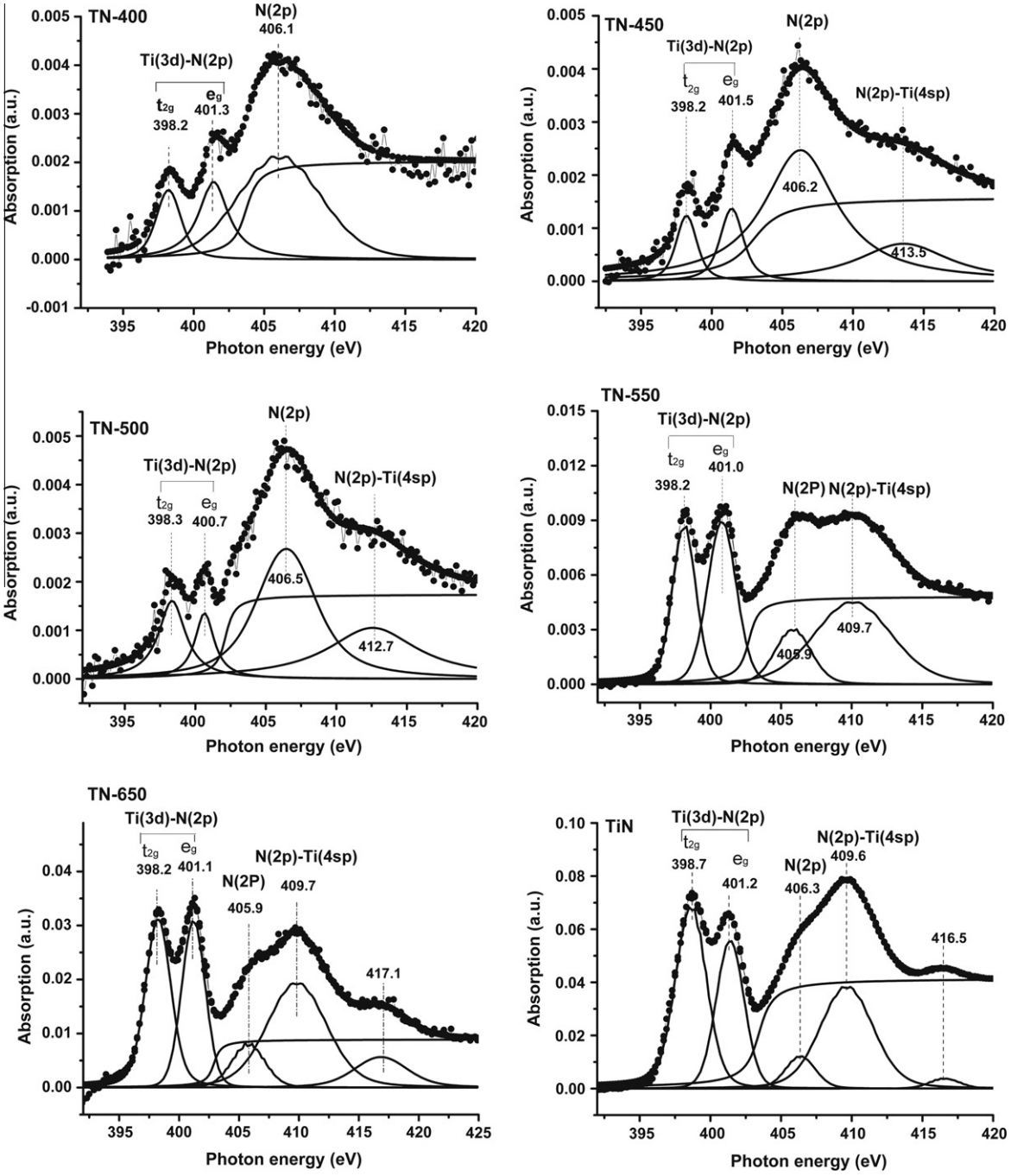

Fig. 13. N 1s NEXAFS spectra with least-squares fit of Viogt functions and Arctan functions.

Table 3
Peak position (eV) of N K-edge features of the TN-*n* samples.

Sample	t_{2g}	e_g	E_{sp}	$\Delta(e_g - t_{2g})$	$\Delta(E_{sp} - t_{2g})$
TN-400	398.2	401.3	–	3.1	–
TN-450	398.2	401.5	413.5	3.3	15.3
TN-500	398.3	400.7	412.7	2.4	14.4
TN-550	398.2	401.0	409.7	2.8	11.5
TN-650	398.2	401.1	409.7	2.9	11.5
TiN	398.7	401.2	409.6	2.5	10.9

from the fit are given in Table 3. In the case of TiN reference, the ligand coordination around each Ti atom is perfect and the t_{2g} and e_g bands split accordingly (Δ = 2.5 eV). It is important to note that the TN-500 sample with highest photocatalytic activity shows almost the same splitting energy (Δ = 2.4 eV) of the t_{2g} and e_g bands as the reference TiN, lower than other N-doped TiO_2 catalysts. Moreover, the TN-500 (398.3 eV) represents a higher energy position of t_{2g} feature compared to other nitrified samples (398.2 eV), indicating a stronger interaction of N 2p–Ti 3d orbitals. In addition, noting that with increasing nitridation temperature, the energy position of [N 2p–Ti 4sp] feature shifts from 413.5 eV for the TN-450 to 412.7 eV for the TN-500 and finally to 409.7 eV for the TN-550 and TN-650 as a result of the strengthened interaction between N 2p and Ti 4sp orbitals. Compared to the TN-500 sample, the [N 2p–Ti 4sp] feature of the TN-550 sample sharply shifts by 3.0 eV toward low energy because of the formation of TiN species shown by the above XPS results. These results give a

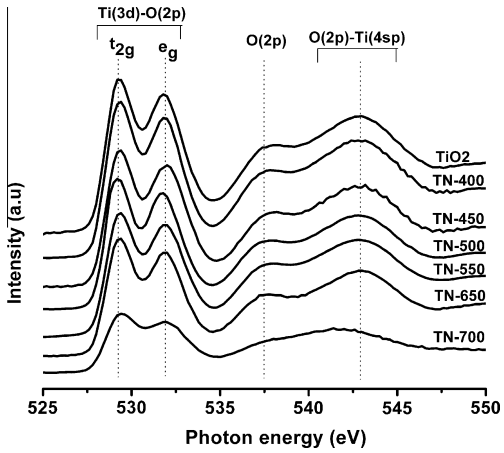

Fig. 14. NEXAFS spectra for the O K-edge of the parent TiO_2 and TN-*n* samples.

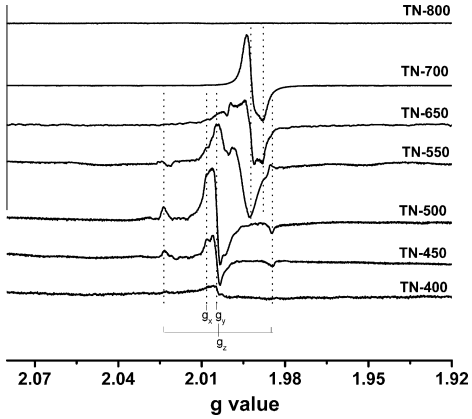

Fig. 15. EPR spectra of the TN-*n* samples at 77 K.

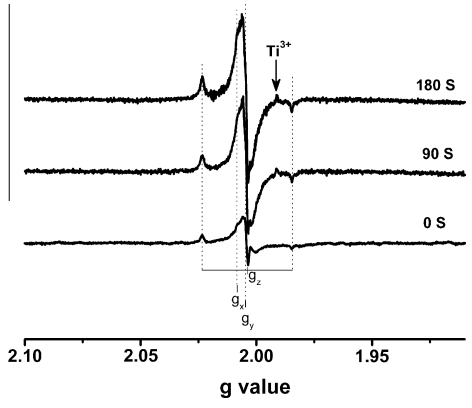

Fig. 16. EPR spectra of the TN-500 sample under vacuum at 77 K with visible light irradiation for different time.

conclusive evidence for the direct bonding of doped N atoms with Ti in these N-doped TiO_2 catalysts.

In addition, we further examined the effect of N dopant on the chemical states of O atoms by analyzing O K-edge NEXAFS of these TN-*n* samples. Fig. 14 displays the O K-edge NEXAFS spectra of the parent TiO_2 and TN-*n* samples. The NEXAFS for the parent TiO_2 is in rather good agreement with the results reported in literature [35]. Two energy regions can be distinguished. The two relatively sharp features in the region from 530 to 535 eV correspond to the

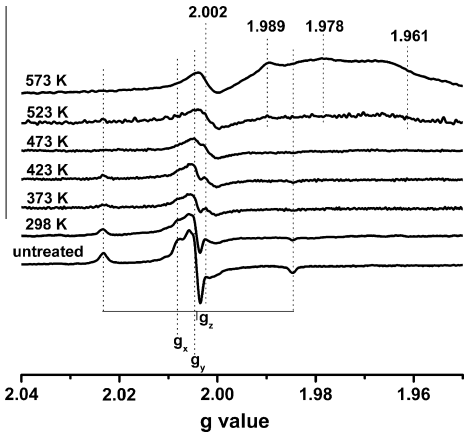

Fig. 17. EPR spectra of the TN-500 sample vacuum degassed at different temperature for 1 h recorded at 77 K.

electron transitions from the O 1s orbital to the t_{2g} (Ti 3d + O 2pπ) and e_g (Ti 3d + O 2pσ) orbitals [34]. This spectral region is very sensitive to local symmetry and ligand coordination. The higher energy broad features between 535 and 547 eV originate from the transitions to hybridized orbitals involving the antibonding orbitals Ti 4sp and O 2p. Evidently, the O K-edge NEXAFS features of all N-doped TiO_2 samples are similar to that of TiO_2, but display a decrease in absorption intensity and become less resolved with increasing nitridation temperature as a consequence of the increase in nitrogen dopant. We used least-squares fit of Voigt functions and Arctan functions to further analyze the t_{2g} and e_g states in the O K-edge NEXAFS spectra (see Fig. S2 in Supporting information). A new e.g. resonance occurs at ca. 531.2 eV and increases gradually in intensity with increasing nitridation temperature, indicating that N doping causes the splitting of the e_g states into d_{z^2} and $d_{x^2-y^2}$. The d_{z^2} and $d_{x^2-y^2}$ orbitals of the e_g states are directed toward oxygen anion and therefore more sensitive to derivations from octahedral symmetry [36]. Consequently, one can be concluded that the N doping distorts octahedral symmetry of TiO_2. This is very consistent with the results reported by Braun et al. [37].

3.6. EPR spectroscopy

Fig. 15 shows the EPR spectra measured at 77 K of the N-doped TiO_2 samples. Upon incorporation of nitrogen in TiO_2 at 400 °C, a set of signals with orthorhombic spectral lines (labeled as A) appear at $g_x = 2.007$, $g_y = 2.005$, and $g_z = 2.004$. The lines A increase markedly in intensity with increasing nitridation temperature and reach a maximum at 500 °C along with a significant decrease and finally disappear at 700 °C. As the EPR spectra of the N-doped TiO_2 samples were recorded at room temperature, the lines A can also be observed clearly (data are not shown inhere). Livraghi et al. [38] observed also the same resonance lines A for N-doped TiO_2 materials at 177 K, whereas the rhombic spectral lines at $g_1 = 2.001$, $g_2 = 1.998$, and $g_3 = 1.927$, belonging to molecular nitric oxide (NO), dominated in the EPR spectra recorded at 77 K. They initially assigned the lines A to the NO_2^{2-} species originated from the reaction of NO gas with O^{2-} ions of TiO_2 [38] and subsequently withdrawn onto NO^{2-} arisen from the interaction of NO gas with an oxygen vacancy [39]. Based on theoretical calculations, Valentin et al. [40] suggested that the assignment of the nitrogen paramagnetic species to a NO_2^{2-} radical ion should be discarded since this species was computed to be unstable in bulk TiO_2. The inconsistent assignment shows that the EPR lines A generated after nitridation have not been fully understood so far in photocatalysis commu-

nity. It is very difficult to identify unambiguously the photoactive N species in only terms of EPR technique, because both substitutional and interstitial nitrogen impurities possess theoretically similar hyperfine coupling parameters [40] and thus present similar EPR lines. In this work, it is interesting to note that the change in the intensity of the lines A with nitridation temperature is in parallel to the amount of the N1 species doped in TiO_2 shown by XPS characterization; one can be thus concluded that the lines A are originated from the N1 species.

Upon nitridation above 500 °C, the intensity of the lines A starts to decrease and a new EPR signal with a shoulder at $g = 1.988$ appears synchronously at $g = 1.992$ and becomes more prominent up to 700 °C. The two EPR lines at $g = 1.992$ and 1.988 are assigned to the bulk Ti^{3+} and the surface Ti^{3+}, respectively [41]. This shows that a part of Ti^{4+} cations including surface Ti^{4+} and bulk Ti^{4+} are reduced by oxygen vacancies created with NH_3 annealing or H_2 arising from the thermal decomposition of NH_3 beyond 550 °C [11]. No any EPR signals are observed for the TN-800 as TiO_2 is transformed into TiN at 800 °C. These EPR results are in good agreement with the XPS and NEXAFS results reported above.

Fig. 16 displays the change in the EPR spectra of the TN-500 catalyst at 77 K in vacuum before and after visible light irradiation. It appears that the intensity of the lines A increases significantly after visible light illumination, followed by the simultaneous occurrence of Ti^{3+} species at $g = 1.988$. This phenomenon is also observed on the TN-400, TN-450 and TN-550 catalysts. Livraghi et al. [21] observed the similar phenomenon that the lines A observed at 298 K in vacuum increase gradually in intensity with irradiation time, but they did not find the corresponding formation of Ti^{3+} under irradiation. Coronada et al. [42] reported that TiO_2 excited by 365-nm UV light also represented the EPR signal of Ti^{3+} at $g = 1.990$ and yet not the EPR lines A. It is certain that the enhancement of the lines A originates from the increase in the paramagnetic N species (designated as N1-1), suggesting that there exists diamagnetic N species (designated as N1-2), which can be excited by visible light to transform into the paramagnetic N1-1 species, in these N-doped TiO_2 materials. The formation of these Ti^{3+} species is mainly because Ti^{4+} traps photoexcited electron from diamagnetic N1-2 species. After irradiation ca. 10 min, the intensity of EPR lines A reaches a platform (see Fig. S3 in Supporting information) and is about four times of no irradiation. It shows that the diamagnetic N1-2 species are predominant in the TN-500 sample.

To further confirm the existence of the diamagnetic N1-2 species and better understand their transformation processes under visible light irradiation, we monitored the change in the EPR spectra of the TN-500 sample after vacuum treatment at different temperatures. As shown in Fig. 17, with increasing treatment temperature, the lines A representing paramagnetic N1-1 species decrease gradually in intensity along with the increase in the intensity of the EPR line of oxygen vacancy at $g = 2.002$. At the same time, the surface N/Ti atomic ratio of the TN-500 sample obtained by XPS analysis still keeps a constant (see Table S2 in Supporting information), while the surface O/Ti atomic ratio is reduced. These results indicate that the heating treatment causes the increase in oxygen vacancies, which makes the paramagnetic N1-1 species transform into the diamagnetic N1-2 species.

4. Discussion

4.1. Local structure and evolution of surface nitrogen species in N-doped TiO_2 catalysts

The post-nitridation of TiO_2 by NH_3 is a step-by-step reaction process. The nitridation takes only place on the surface layer and sublayer of TiO_2 below 500 °C. A XPS etching experiment reveals that the N species disappear completely when the TN-500 sample was etched to ca. 10 nm of depth, which validates that N atoms are present only on the surface of TiO_2. A transitional temperature region from the surface-nitrified layer containing N to the separated TiN nanoparticles exists in the range of 500–650 °C. The TEM and XRD results indicate that above 550 °C, N atoms replace O atoms to form the crystalline phase of TiN as N2 species, while the nitrified samples below 500 °C maintain the original crystal phase of TiO_2. The desirable nitridation temperature is established to be at 500 °C, where the obtained N-doped TiO_2 catalyst shows excellent visible light activity for the oxidation of acetone. The N atoms doped in these N-doped TiO_2 samples prepared below 500 °C are not present as TiN species, but highly dispersed in the surface layer as N1 species.

Based on the XPS characterization results, it can be concluded that the N1 species with a binding energy of ca. 399.6 eV are related with the visible light activity, while the N2 species with a binding energy of ca. 396 eV representing TiN species are deleterious to the visible light photocatalysis. The latter can be assigned unambiguously to N^{3-} species directly bonded to three Ti^{3+} cations in light of the binding energy similar to that of TiN as described in Scheme 1A, whereas the assignment to the former is not so straightforward. Asahi et al. [3] also observed the N1 species with a binding energy of 400 eV and assigned it to molecularly chemisorbed γ-N_2, whereas Sato et al. [14] disagreed to the assignment and suggested that it should be attributed to N similar to NO that is not bound directly to Ti. Oliver et al. [18] used XPS spectroscopy to study *in situ* the nitrogen doping over TiO_2 (1 1 0) single crystal under NH_3 gas stream at 870 K and proposed that the N 1s XPS peak occurring at ~400 eV belongs to NH_x species doped in interstitial site. Chen and Burda [17] ascribed the N 1s peak at ~400 eV to O–Ti–N species. Although the assignment to the N1 species has been controversial, a typical understanding, the N 1s XPS peak appearing at ca. 400 eV is assignable to N species doped in oxygen vacancies or interstitial sites, is acceptable.

Our EPR results indicate that the N1 species consist of the paramagnetic N1-1 species and the diamagnetic N1-2 species. For the geometric structure of the N1-1 species, there are five kinds of structures suggested in literatures [30,40], as described in Scheme 1. The model B proposed by Oliver et al. [18] described one imino-type species, which may be created by the incomplete reaction of NH_3 with surface oxygen atoms. Based on SSNMR and EPR characterization results, Raftery et al. [15] believed that the photoactive nitrogen species should be nitrate-type species (Model C), which are converted from imino species (Model B). Nitrogen atom in the model B is linked directly with oxygen anions of the TiO_2 lattice. For our samples, the models B and C can be completely ruled out in light of three facts: (i) no H hyperfine EPR lines of NH_x species were observed (excluding model B); (ii) there exists a direct

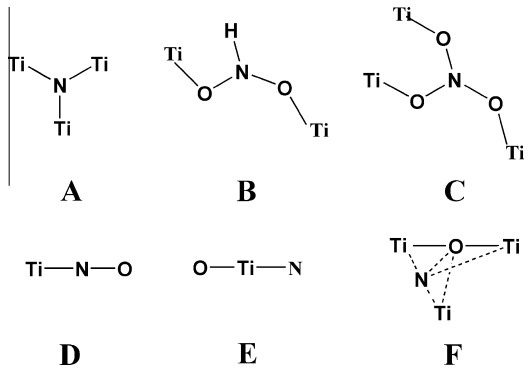

Scheme 1. Structural models of N species in N-doped TiO_2 samples reported in literatures [15–18,30,40].

orbital interaction between nitrogen dopant and Ti cations as indicated by the NEXAFS results (excluding model C); (iii) N doping leads simultaneously to the splitting of the e_g states as shown by the NEXAFS results. The Ti–N–O (model D) only occurs in the TN-650 and TN-700 samples, as indicated by the N 1s peak at ca. 397.0 eV and the Ti 3d peak at ca. 457.0 eV. As for the model E suggested by Chen and Burda [17] (i.e. nitrogen replaces the lattice oxygen atom of O–Ti–O–Ti to form O–Ti–N–Ti during the doping process) and the model F, they can well explain the above three facts. Owing to the reduced electron density of N by the O atom, the N 1s binding energy in the O–Ti–N environment is higher than that in an N–Ti–N environment. Moreover, because the atomic radius of N is larger than that of O, the N doped at oxygen vacancy will cause the distortion of octahedral TiO_4 units. Consequentially, the strong orbital interaction between N and neighboring O atoms in an octahedral [TiO_3N] unit leads to the splitting of the [Ti 3d + O 2pπ] hybrided states. Although the interstitial N dopant for the model F is not bound to Ti^{4+} cations, it interacts simultaneously with vicinal Ti and O atoms. This will make their molecular orbits partly overlap, resulting in the increase in electron density, as reflected from the NEXAFS spectra showing the direct bonding of N to Ti cation and the XPS spectra showing the gradual decrease in the O 2p and Ti 3d binding energy with increasing N content. Therefore, it can be deduced preliminarily that the paramagnetic N1-1 species may be present in the form of the model E or F. Which is it? This must be dependent on the identification of the diamagnetic N1-2 species. According to the EPR result that the visible light irradiation induces the diamagnetic N1-2 species to transform into the paramagnetic N1-1 species, we proposed that the photoactive N1-2 species should be a [$O–Ti^{4+}–N^{3-}–Ti^{4+}–V_0^-$] cluster containing an oxygen vacancy and a N atom, as shown in Scheme 2. Under visible light irradiation, the diamagnetic single N^{3-} in the structural model can be excited to form paramagnetic N^{2-}. The photoexcited electron is transferred to Ti^{4+} atom, leading to the formation of Ti^{3+}. The structural model can well explain all characterization data including XPS results (i.e. the valence state of the N1 species is between −2 and −3 and the 1s binding energy of the N1 species decreases with increasing nitridation temperature as a result of the electron-donating effect of oxygen vacancy formed during incorporation) and the NEXAFS results (i.e. N species are directly bound to Ti^{4+} cations). Based on the similar geometric environment of the single N atom in the photoexcited N1-2 species and the model E, one can be further ensured that the paramagnetic N1-1 species should be $O–Ti^{4+}–N^{2-}–Ti^{4+}$ (model E), instead of the interstitial N with structure of the model F.

The saturation concentration of the N1 species in our samples is found to be 0.23 wt.%, lower than the value reported in literature (1–6%, molar ratio) [3,17,18]. This is mainly because only surface-layer TiO_2 was nitrified by NH_3 below 500 °C. When nitridation temperature is beyond 500 °C, the N1 species decrease quickly along with the increase in TiN species. It shows that the N1 species are altered into TiN species. This structural transformation may be originated mainly from excessive oxygen vacancies that create more easily in the N-doped TiO_2 [40]. High nitridation temperature (above 500 °C) can make the electrons of oxygen vacancies transfer to Ti^{4+} cations, leading to the formation of Ti^{3+} states. The EPR results (Fig. 15) prove that the defect sites (Ti^{3+} cations) including both inner Ti^{3+} ($g = 1.992$) and surface Ti^{3+} ($g = 1.988$) begin to appear in N-doped TiO_2 at 550 °C. It seems that a phase transition from TiO_2 to TiN is closely associated with lattice distortion, reduction of Ti^{4+} to Ti^{3+}, and finally structural reconstruction. The progressive change in the higher energy broad features of O K-edge NEXAFS spectra confirms the structural distortion of TiO_2 during N doping process.

4.2. Nature of visible light photocatalysis of N-doped TiO_2

The present explanation for the light response and visible light photocatalysis of N-doped TiO_2 is mainly based on the classical semiconductor theory, which only offers an abstract demonstration for the photoexcitation of catalysts (i.e. photogenerated electrons jump from valence band to conduction band). However, it is helpless for describing a photocatalysis that is essentially a photochemical process. For example, in the homogeneous photocatalytic reaction system [43–45], there occurs an intramolecular charge transfer of catalyst under light irradiation, i.e. the chromophore of catalyst absorbs light to produce a high-energy excited state that can activate reactants or directly oxidize reactants. This photoinduced charge transfer was extensively applied to explain the photocatalytic behavior taking place over zeolite-based photocatalysts containing metal-oxo centers [46,47]. Surprisingly, the photochemical behavior also occurs on N-doped TiO_2 under visible light irradiation, as indicated by the charge transfer between Ti^{4+} and N^{3-} observed by EPR (Fig. 16). Livraghi et al. [21] observed also that when N-doped TiO_2 was irradiated in oxygen atmosphere by more than 420-nm visible light, the photogenerated electron from the nitrogen impurities can be transferred to O_2 to produce surface superoxide O_2^- radical. Therefore, it can be concluded that the substitutional nitrogen species with a diamagnetic [$O–Ti^{4+}–N^{3-}–Ti^{3+}–V_0^-$] core are the photoactive

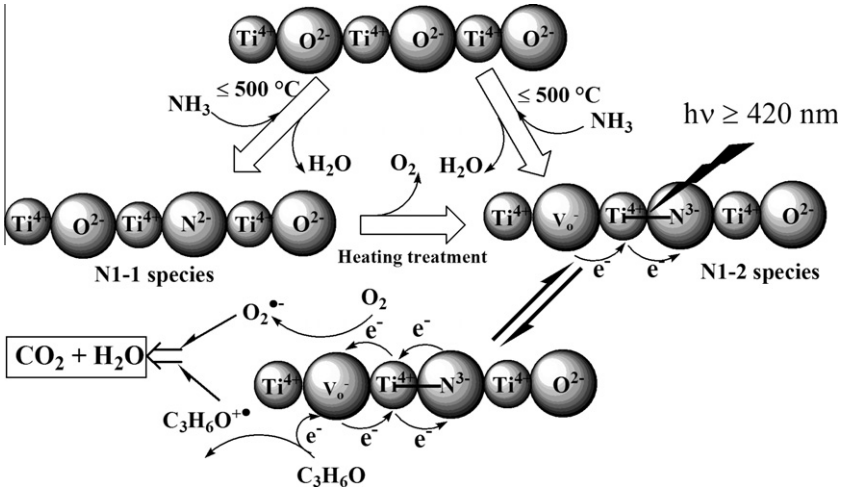

Scheme 2. Structural models of N1 species and suggested mechanism for the photocatalysis.

centers as a source for the photogenerated electron transfer to reducible adsorbates like O_2.

N1/Ti atomic ratio has a near linear correlation with conversion of acetone (Fig. 9). It confirms that the substitutional N1 species are closely related with the visible light photocatalysis of N-doped TiO_2. However, the optical absorption derived from the bandgap narrowing by N substitutional doping of TiO_2 is inconsistent with photocatalytic activity, as pointing out by some authors [11,48]. The UV–vis DRS results (Fig. 7B) indicate that the absorption band of visible light region increases rapidly in intensity with increasing nitridation temperature from 400 to 550 °C, but such an increase is not in parallel to their visible light photoactivity. A dramatic drop in the photoactivity occurred at 550 °C, clearly indicating no correlation between absorption features and photocatalytic activity. Moreover, the TN-400 sample shows a gradual increase in photoactivity within 10 h of nitridation time and finally reaches a constant with further increasing nitridation time (Fig. 1), while the intensity of the absorption band is continuously enhanced (Fig. 6). This further indicates no intrinsical correlation between the absorption features and the photocatalytic activity of N-doped TiO_2. As mentioned above, nitridation of TiO_2 not only leads to nitrogen doping but also to the formation of defects including oxygen vacancies and Ti^{3+} states, which are all contributing to visible light absorption features. Oxygen vacancies and Ti^{3+} states were reported to strongly influence photocatalytic activity by acting as charge carriers trapping and/or recombination centers by themselves or through a impurity–vacancy electronic interaction [40,48].

A synergistic effect of N dopant and oxygen vacancies in TiO_2 maybe contributes to the great enhancement of the visible light photoactivity. For the nitrogen atom doping in TiO_2 lattice, the occupied N 2p localized states induce the redshift of the optical absorption edge toward lower light energy, as indicated by an additional absorption shoulder in the visible light region centered at about 430 nm. The oxygen vacancy state in TiO_2 below the lower end of the conduction band at 0.75–1.18 eV also partly contributes to the extension of the light absorption from UV to visible. Obviously, these oxygen vacancies can act as electron–hole recombination centers under UV light illumination, leading to the decrease in the UV light photocatalytic activity. This is verified by the results reported in Section 3.2 and the previous studies [11,14,23,24]. However, under visible light irradiation, the surface $O–Ti^{4+}–N^{3-}–Ti^{4+}–V_0^-$ species, instead of bulk TiO_2, are excited to produce an excited state of $[O–Ti^{4+}–N^{2-}–Ti^{3+}–V_0^-]^*$, as shown by EPR spectra (Fig. 16). As special electron–hole pair states, the $[O–Ti^{4+}–N^{2-}–Ti^{3+}–V_0^-]^*$ activates O_2 and acetone molecules, leading to the oxidation of acetone into CO_2 and H_2O, as shown in Scheme 2.

5. Conclusions

The following conclusions may be drawn from the present work: (1) The post-nitridation of TiO_2 by NH_3 commonly causes the heterogeneous distribution of N atoms in the surface layer of TiO_2 nanoparticles. The nitridation temperature affects considerably the chemical states and content of nitrogen species doped in TiO_2. The optimal nitridation temperature was found to be 500 °C, where the obtained N-doped TiO_2 catalyst shows a better photocatalytic activity for the oxidation of acetone under visible light irradiation. (2) The combined characterization results of multiple spectroscopic techniques reveal that four kinds of N species appear alone or together in N-doped TiO_2, dependent on nitridation temperature. Low nitridation temperature (below 500 °C) results in a small amount of N doped in TiO_2 in the two forms of substitutional N species as described in Scheme 2. Other two types of photocatalytically inert N species as described by the models A and D only occur in the case of high nitration temperature (above 550 °C). (3) The visible light photoactive centers of N-doped TiO_2 were identified unambiguously to be the substitutional N species with a diamagnetic $[O–Ti^{4+}–N^{3-}–Ti^{4+}–V_0^-]$ cluster containing an oxygen vacancy and a N atom, which acts as a source for the photogenerated electron transfer to reducible adsorbates like oxygen. After excitation by visible light, the diamagnetic N^{3-} species can be transformed into paramagnetic N^{2-} species by the charge transfer, followed by the appearance of Ti^{3+}. (4) The photoexcited mechanism of N-doped TiO_2 should be based on a surface excited state of the $[Ti^{4+}–N^{3-}]$ unit. A synergistic effect of N dopant and oxygen vacancy in TiO_2 contributes to the great enhancement of the visible light photoactivity. (5) In summary, this study demonstrates a general picture that the chemical states, structural evolvement, and distribution of N dopant in TiO_2 gain a deeper understanding of the nature of visible light photocatalysis of N-doped TiO_2 catalysts. This work offers a reference route for the study of photoactive centers of other ions-doped photocatalysts.

Acknowledgments

This work was financially supported by the National Natural Science Foundation of China (Grant Nos. 21003021, 20673020, 20873022), National Basic Research Program of China (973 Program, No. 2007CB613), the National High Tech R&D Program of China (863 Program, 2008AA06Z326), the Natural Science Foundation of Fujian Province of PR China (2010J05024), and Programs for Changjiang Scholars and Innovative Research Team in University (PCSIRT0818) and for New Century Excellent Talents in University (XSJRC2007–19), Fujian Province of PR China. The authors are very grateful for Dr. Wensheng Yan and Feng Wang, Hefei Synchrotron Radiation Laboratory (NSRL) (University of Science and Technology of China, Hefei) for the collection, discussion, and analysis of NEXAFS data.

Appendix A. Supplementary material

Supplementary data associated with this article can be found, in the online version, at doi:10.1016/j.jcat.2010.07.033.

References

[1] M.R. Hoffmann, S.T. Martin, W. Choi, D.W. Bahnemann, Chem. Rev. 95 (1995) 69.
[2] J.H. Park, S. Kim, Allen.J. Bard, Nano Lett. 6 (2006) 24.
[3] R. Asahi, T. Morikawa, T. Ohwaki, K. Aoki, Y. Taga, Science 293 (2001) 269.
[4] M. Anpo, M. Takeuchi, J. Catal. 216 (2003) 505.
[5] A. Fujishima, X. Zhang, D.A. Tryk, Surf. Sci. Rep. 63 (2008) 515.
[6] W. Zhao, W. Ma, C. Chen, J. Zhao, Z. Shuai, J. Am. Chem. Soc. 126 (2004) 4782.
[7] H. Wang, J.P. Lewis, J. Phys. Condens. Matter. 18 (2006) 421.
[8] G. Xiao, X. Wang, D. Li, X. Fu, J. Photochem. Photobiol. A: Chem. 193 (2008) 213.
[9] H. Huang, D. Li, Q. Lin, W. Zhang, Y. Shao, Y. Chen, M. Sun, X. Fu, Environ. Sci. Technol. 43 (2009) 4164.
[10] S.U.M. Khan, M. Al-Shahry, W.B. Ingler Jr., Science 297 (2002) 2243.
[11] H. Irie, Y. Watanabe, K. Hashimoto, J. Phys. Chem. B 107 (2003) 5483.
[12] M. Sathish, B. Viswanathan, R.P. Viswanath, C.S. Gopinath, Chem. Mater. 17 (2005) 6349.
[13] J.L. Gole, J.D. Stout, C. Burda, Y. Lou, X. Chen, J. Phys. Chem. B 108 (2004) 1230.
[14] S. Sato, R. Nakamura, S. Abe, Appl. Catal. A: Gen. 284 (2005) 131.
[15] E.A. Reyes-Garcia, Y. Sun, K. Reyes-Gil, D. Raftery, J. Phys. Chem. C 111 (2007) 2738.
[16] C. Belver, R. Bellod, A. Fuerte, M. Fernandez-Garcia, Appl. Catal. B: Environ. 65 (2006) 301.
[17] X. Chen, C. Burda, J. Phys. Chem. B 108 (2004) 15446.
[18] O. Diwald, T.L. Thompson, T. Zubkov, E.G.O. Goralski, S.D. Walck, J.T. Yates, J. Phys. Chem. B 108 (2004) 6004.
[19] N. Serpone, J. Phys. Chem. B 110 (2006) 24287.
[20] X. Chen, X. Wang, Y. Hou, J. Huang, L. Wu, X. Fu, J. Catal. 255 (2008) 59.
[21] S. Livraghi, M.C. Paganini, E. Giamello, A. Selloni, C.D. Valentin, G. Pacchioni, J. Am. Chem. Soc. 128 (2006) 15666.
[22] K. Suriye, P. Praserthdam, B. Jongsomjit, Appl. Surf. Sci. 253 (2007) 3849.
[23] M. Miyauchi, A. Ikezawa, H. Tobimatsu, H. Irie, K. Hashimoto, Phys. Chem. Chem. Phys. 6 (2004) 865.
[24] T.L. Thompson, J.T. Yates Jr., Top. Catal. 35 (2005) 197.

[25] D. Li, H. Haneda, N.K. Labhsetwar, S. Hishita, N. Ohashi, Chem. Phys. Lett. 401 (2005) 579.
[26] I. Nakamura, S. Negishi, S. Kutsuna, T. Ihara, S. Sugihara, K. Takeuchi, J. Mol. Catal. A 161 (2000) 205.
[27] X. Chen, Y.B. Lou, A.C.S. Samia, C. Burda, J.L. Gole, Adv. Funct. Mater. 15 (2005) 41.
[28] J.F. Moulder, W.F. Stickle, P.E. Sobol, K.D. Bomben, Handbook of X-Ray Photoelectron Spectroscopy, Physical Electronic, Inc., USA, 1992. p. 42.
[29] N.C. Saha, H.G. Tompkins, J. Appl. Phys. 72 (1992) 3072.
[30] E. György, A. Pérez del Pino, P. Serra, J.L. Morenza, Surf. Coat. Technol. 173 (2003) 265.
[31] H. Li, J. Li, Y. Huo, J. Phys. Chem. B 110 (2006) 1559.
[32] M.J. Tarlov, J.F. Evans, J. Vac. Sci. Technol. A 5 (1987) 941.
[33] H. Chen, A. Nambu, W. Wen, J. Graciani, Z. Zhong, J.C. Hanson, E. Fujita, J.A. Rodriguez, J. Phys. Chem. C 111 (2007) 1366.
[34] J.G. Chen, Surf. Sci. Rep. 30 (1997) 1.
[35] V.S. Lusvardi, M.A. Barteau, J.G. Chen, J.J. Eng, A. Teplyakov, B. Fruhberger, Surf. Sci. 397 (1998) 237.
[36] L. Soriano, M. Abbate, J.C. Fuggle, C. Jiménez, J.M. Sanz, L. Galán, C. Mythen, H.A. Padmore, Surf. Sci. 281 (1993) 120.
[37] A. Braun, K.K. Akurati, G. Fortunato, F.A. Reifler, A. Ritter, A.S. Harvey, A. Vital, T. Graule, J. Phys. Chem. C 114 (2010) 516.
[38] S. Livraghi, A. Votta, M.C. Paganini, E. Giamello, Chem. Commun. (2006) 498.
[39] S. Livraghi, M.R. Chierotti, E. Giamello, G. Magnacca, M.C. Paganini, G. Cappelletti, C.L. Bianchi, J. Phys. Chem. C 112 (2008) 17244.
[40] C.D. Valentin, G. Pacchioni, A. Selloni, S. Livraghi, E. Giamello, J. Phys. Chem. C 109 (2005) 11414.
[41] C.P. Kumar, N.O. Gopal, T.C. Wang, M.S. Wong, S.C. Ke, J. Phys. Chem. B 110 (2006) 5223.
[42] J.M. Coronado, A.J. Maira, J.C. Conesa, K.L. Yeung, V. Augugliaro, J. Soria, Langmuir 17 (2001) 5368.
[43] S. Kim, H. Park, W. Choi, J. Phys. Chem. B 108 (2004) 6402.
[44] P. Du, K. Knowles, R. Eisenberg, J. Am. Chem. Soc. 130 (2008) 12576.
[45] M. Imanishi, K. Hashimoto, H. Kominami, Chem. Lett. 39 (2010) 352.
[46] M. Matsuoka, M. Anpo, J. Photochem. Photobiol. C 3 (2003) 225.
[47] G. Yan, J. Long, X. Wang, Z. Li, X. wang, Y. Xu, X. Fu, J. Phys. Chem. C 111 (2007) 5495.
[48] C. Belver, R. Bellod, S.J. Stewart, F.G. Requejo, M. Fernandez-Garcia, Appl. Catal. B: Environ. 65 (2006) 309.